Journal of Materials Science: Materials in Electronics (2020) 31:5948–5957
https://doi.org/10.1007/s10854-020-03203-2

CNT anchored by $NiCo_2O_4$ nanoparticles with hybrid structure for ultrahigh-performance supercapacitor

Weiguo Zhang[1] · Jinlong Xu[1] · Hongzhi Wang[1] · Suwei Yao[1]

Received: 10 November 2019 / Accepted: 3 March 2020 / Published online: 13 March 2020

Abstract
One-dimensional carbon nanotube material decorated by $NiCo_2O_4$ nanoparticles has been successfully fabricated by a facile one-pot hydrothermal method together with a sequent annealing treatment. The as-prepared nanoscale CNT-$NiCo_2O_4$ composites with network structure manifested an enhanced specific capacitance of 1055A g^{-1} at a current density of 1 A g^{-1} and an outstanding cycling performance compared with pure $NiCo_2O_4$. When tested at current density of 20 A g^{-1}, excellent capacity retention ratio up to 99.8% can be achieved for the composite electrode after 6500 cycles. The remarkable cycling performance can mainly be attributed to composite unique structure that CNTs present high conductivity together with $NiCo_2O_4$ nanoparticle's eminent capacity. Consequently, the ultrahigh specific capacity coupled with admirable cycling stability makes such composite a promising electrode material candidate for supercapacitor in energy storage.

1 Introduction

The ever-growing energy depletion of fossil fuels and increasing environmental pollution have stimulated the exploration of new energy-storage devices for researchers all over the world to fulfill the purpose of clean, efficient, and sustainable [1, 2]. Supercapacitors, also called electrochemical capacitors, have been considered as one of the most promising energy conversion/storage systems due to their many interests, containing higher power density, low maintenance coupled with longer lifespan over batteries, and higher energy density and cycling stability compared with conventional electrostatic capacitors [3–6]. The performance of supercapacitors is largely influencing by the structure, morphology, and species of the electrode materials [7, 8]. Transition metal oxides, as one of the most promising supercapacitor electrode materials, have many excellent advantages such as abundant, low cost, and environmentally friendly, which attract an increasing number of researcher's attention [9, 10]. Among metal oxides, a binary spinel metal oxide $NiCo_2O_4$ is an excellent electrode material for the supercapacitors owing to its high stability, environmental friendliness, and abundant resources [11, 12]. However, the conductivity of nickel cobaltite is poor, which could substantially decrease the practical specific capacitance of nickel cobaltite $NiCo_2O_4$ compared with more than 3000 F g^{-1} theoretical value [13, 14]. To address this problem, the integration of ternary nanosize oxides $NiCo_2O_4$ with conductive substrates is an efficient method.

Carbon materials, such as carbon nanotubes (CNTs), carbon black, and graphene, are the most important electrode material [15, 16]. Although graphene has good conductivity, its cyclic stability is poor compared with CNTs [17]. It is noting that CNT, as an electrode material of conventional electrical double-layer capacitors, is generally considered as promising electrode material candidates for the supercapacitor because of their remarkable chemical stability, very large specific area, lightweight, and outstanding conductivity [18, 19]. However, the specific capacitance of CNT is typically limited by the fact of reversibly adsorbing charge storage mechanism at the surface of electrode/electrolyte interface [20]. To solve this problem, researchers combine various kinds of transition metal oxides with graphene or CNT to improve the electrochemical performance of supercapacitor [21–30]. Table 1 shows material, specific capacitance, rate capability, cycle stability of CNT, and graphene-based as well as pure $NiCo_2O_4$ electrode material. The result

Electronic supplementary material The online version of this article (https://doi.org/10.1007/s10854-020-03203-2) contains supplementary material, which is available to authorized users.

✉ Hongzhi Wang
wanghz@tju.edu.cn

[1] Department of Applied Chemistry, School of Chemical Engineering and Technology, Tianjin University, Tianjin 300350, People's Republic of China

Table 1 Electrochemical performance of different electrode materials

Material	Specific capacitance (F g^{-1})	Rate performance	Capacity retention	References
CNT@$NiCo_2O_4$	1038 F g^{-1} (0.5 A g^{-1})	64% (10 A g^{-1})	Almost 100% (2 A g^{-1}, 1000 cycles)	[21]
MCNT/GO/$NiCo_2O_4$	707 F g^{-1} (2.5 A g^{-1})	58% (8 A g^{-1})	88% (8 A g^{-1}, 5000 cycles)	[22]
rGO/ $NiCo_2O_4$	1003 F g^{-1} (1 A g^{-1})	89% (10 A g^{-1})	57% (10 A g^{-1}, 10,000 cycles)	[23]
CNTs/C/$NiMoO_4$	1037 F g^{-1} (1 Ag^{-1})	69% (10 A g^{-1})	96.5% (2 A g^{-1}, 1500 cycles)	[24]
CNTs@$NiCo_2O_4$	210 F g^{-1} (2 A g^{-1})	73.2% (50 A g^{-1})	92.7% (2 A g^{-1}, 2500 cycles)	[25]
Co_3O_4@CNTs/PIn	442.5 F g^{-1} (1 A g^{-1})	84% (20 A g^{-1})	90.2% (10 A g^{-1}, 5000 cycles)	[26]
$NiCo_2O_4$/CNT	828 F g^{-1} (1 A g^{-1})	79% (20 A g^{-1})	99% (5 A g^{-1}, 3000 cycles)	[27]
$NiCo_2O_4$ nanoparticles	720 F g^{-1} (1 A g^{-1})	66.3% (20 A g^{-1})	97.3% (20 A g^{-1}, 2000 cycles)	[28]
MnO_2@ $NiCo_2O_4$	684 F g^{-1} (2 A g^{-1})	87.72 (15 A g^{-1}	85.6% (6 A g^{-1}, 4000 cycles)	[29]
CNT@WO_3	496 F g^{-1} (0.5 A g^{-1})	82% (10 A g^{-1})	96.3% (100 mV/s, 8000 cycles)	[30]
$NiCo_2O_4$-CNT	1055 F g^{-1} (1 A g^{-1})	90% (20 A g^{-1})	99.8% (20 A g^{-1}, 6500 cycles)	This work

demonstrates that using above methods, prepared composites have achieved certain effect. However, the effect can further be enhanced.

Based on the above consideration, in this work, we fabricated CNT-$NiCo_2O_4$ composite via a particular one-pot hydrothermal method. Specifically, the unique surfactant (sodium dodecyl sulfate) is used to handle multi-walled carbon nanotube (MWCNT). The method increased hydrophilicity and activity of carbon nanotube, which increased the compounding of CNT and $NiCo_2O_4$. The treated CNT anchored by $NiCo_2O_4$ nanoparticles forms an excellent performance electrode material. The electrochemical test of composite indicates ultrahigh specific capacitance and considerable rate of capability compared with pure $NiCo_2O_4$ electrode material. This is mainly attributed to the close contact between carbon nanotube and nickel cobalt oxide, which provides good electrical conductivity and enables the capacity of $NiCo_2O_4$ to be realized.

2 Experimental section

2.1 Materials fabrication

All used reagents were in the grade of analysis. In a typical synthesis method, 0.5 mg mL^{-1} MWCNT was mixed with different amounts of sodium dodecyl sulfate solution(SDS) (36 mg mL^{-1}, 18 mg mL^{-1} and 0 mg mL^{-1}) and then MWCNT was uniformly dispersed by ultrasonication to obtain high dispersive solution. The prepared solution was mixed with 0.075 mol L^{-1} $Co(NO_3)_2{\cdot}6H_2O$, 0.0375 mol L^{-1} $Ni(NO_3)_2{\cdot}6H_2O$ as well as 0.25 mol L^{-1} urea. Subsequently, the solution received 30 min vigorous stirring at ambient temperature to prepare a black solution. We transferred the resultant solution into the Teflon-lined stainless steel autoclave (100 mL) as well as maintained them in an electric oven for 5 h at 150 °C. The precipitate at the bottom was gathered and purified water together with absolute ethyl alcohol was used to wash them for several circles by high-speed centrifugation, which then received drying treatment at 55 °C. At last, the precursor underwent 3 h annealing at 300 °C at a slow heating rate (1 °C min^{-1}) for the formation of CNT-$NiCo_2O_4$ composite.

For comparison, the pure $NiCo_2O_4$ powder was also synthesized by using the identical situations but without the addition of MWCNT powder. Figure 1 displays the synthesis process of the CNT-$NiCo_2O_4$ samples.

2.2 Materials characterization

The powder X-ray diffraction (XRD) helped to characterize the sample regarding the crystal structure by virtue of a Cu Kα radiation ($\lambda = 1.54056$ Å) with 2θ in the range of 10°–80° at a certain scanning speed (at 5 min^{-1}). Raman analysis was tested using a Raman spectroscopy (Thermo DXR) with a 532 nm excitation laser. X-ray photoelectron spectra (XPS) had been executed on PHI 1600 photoelectron spectrometer equipped with Al Ka radiation ($h\nu = 1486.6$ eV). The transmission electron microscopy (TEM) (JEM 3100F JEOL, Japan) together with the field emission scanning electron microscopy (FESEM) (Hitachi S4800, Japan) helped to characterize the microstructure as well as morphology of as-prepared products.

2.3 Electrochemical measurements

The test on electrochemical property (CHI 660B electrochemical workstation) was carried out in mode with three electrodes using 3 M KOH as the electrolyte, the platinum wire is the counter-electrode, and the saturated calomel electrode (SCE) is the reference electrode. The mixture of as-synthesized samples, polytetrafluoroethylene, as well as acetylene black in the mass ratio of 80:10:10 in absolute ethyl alcohol helped to fabricate the studying electrode,

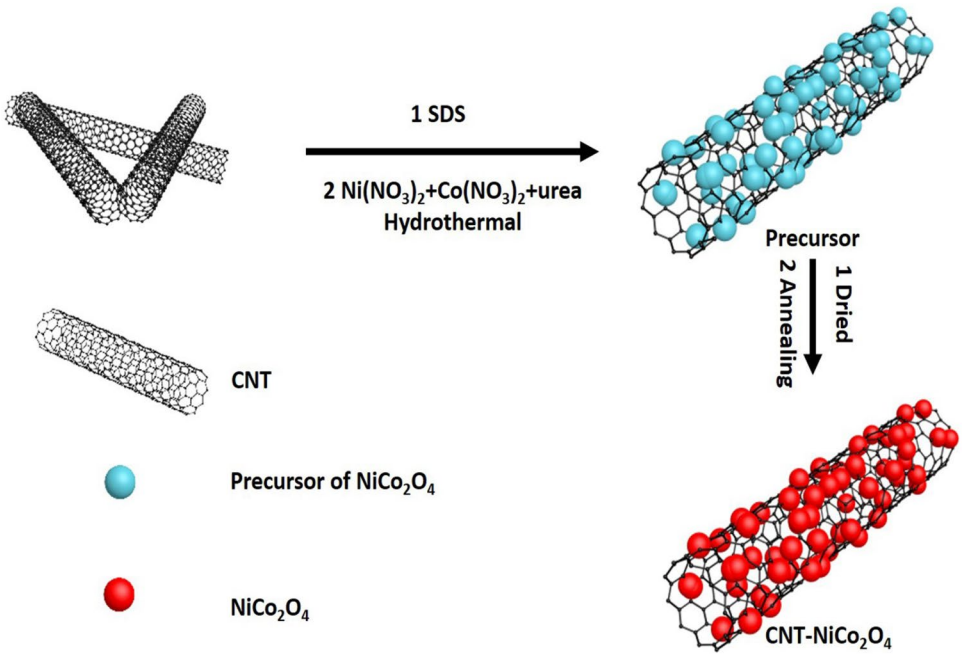

Fig. 1 Schematic illustration of the preparation processes of CNT-$NiCo_2O_4$ composites

which was pasted onto a nickel foam (NF) current collector. Subsequently, the NF substrates underwent drying treatment in a vacuum oven at 40 °C and 10 MPa pressure. Electrochemical tests contain electrochemical impedance spectroscopy (EIS), galvanostatic charge–discharge (GCD), as well as Cyclic voltammetry (CV). The measurement of the CV was performed with the scanning rate at 5 mV s^{-1}, 10 mV s^{-1}, 20 mV s^{-1}, 30 mV s^{-1}, 40 mV s^{-1} , and 50 mV s^{-1} in the range of 0–0.4 V against SCE. GCD curve was drawn under different current densities (1–20 A g^{-1}) in the range of 0–0.4 V. EIS was measured at an open circuit potential, with the frequency changing from 100 kHz to 0.01 Hz with 5 mV AC perturbation. GCD techniques helped to measure the cycle performance on the LAND CT2001A system.

3 Results and discussion

3.1 Morphology and structure characterization

Figure 2a demonstrates the CNT-$NiCo_2O_4$, pure $NiCo_2O_4$, and CNT in terms of their XRD pattern, respectively. In the XRD patterns of CNT, 26° is attributed to a typical diffraction peak considering crystalline graphitic (002) plane of CNT [31]. In the XRD patterns of pure $NiCo_2O_4$ sample, the XRD pattern shows the characteristic peaks at 18.9°,

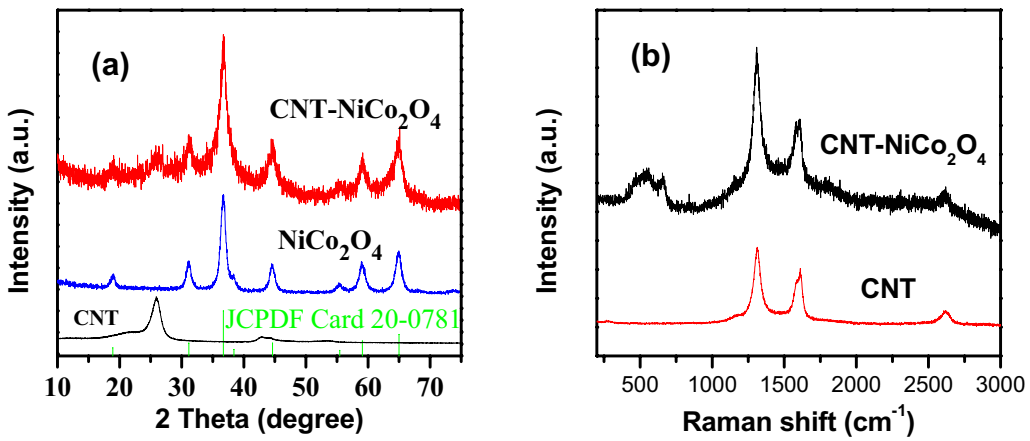

Fig. 2 **a** XRD patterns of samples, **b** Raman spectra of the CNT and CNT-$NiCo_2O_4$ composites

31.2°, 36.7°, 44.7°, 59.0°, and 65.1° according to JCPDS Card No. 20–0781, which can be indexed to the (111), (220), (311), (400), (511), and (440) crystal planes of spinel-type $NiCo_2O_4$, respectively [32]. In conclusion, all the primary diffraction of CNT and pure $NiCo_2O_4$ can be discovered in the patterns of CNT-$NiCo_2O_4$. Besides, no extra diffraction peak can be detected, manifesting the high purity of as-prepared CNT-$NiCo_2O_4$ samples.

Figure 2b shows Raman spectra of CNT and CNT-$NiCo_2O_4$. The spectrum of CNT saw three typical Raman bands: D band at 1354 cm^{-1}, G band at 1578 cm^{-1}, and G_0 band at 2690 cm^{-1}. D bands are attributed to the characteristic feature of disordered graphite or crystal defects, while G and G_0 bands are ascribed to graphitic planes [33]. The intensity ratio of both bands (I_D/I_G) indicated the degree of disorder for carbon materials. According to Fig. 2b, I_D/I_G ratios increased from 1.36 to 1.42 (1.36 for the CNT and 1.42 for the CNT-$NiCo_2O_4$), suggesting an increase of defects for carbon structure in CNT-$NiCo_2O_4$, which might result from the anchoring of $NiCo_2O_4$ nanoparticles on the surface of CNT [34]. Furthermore, the typical peaks at 483 cm^{-1} and 670 cm^{-1} are associated with F_{2g} and A_{1g} vibrational modes of $NiCo_2O_4$, which also can be observed. Considering the above discussions, it further confirms the combination of CNT and $NiCo_2O_4$ nanoparticles [35].

The X-ray photoelectron spectroscopy (XPS) was applied for analyzing more detailed chemical oxidation states of the CNT-$NiCo_2O_4$ nanoparticle and the corresponding results are displayed in Fig. 3. An entire survey on CNT-$NiCo_2O_4$ shows the existence of C 1 s, O 1 s, Co 2p, and Ni 2p (Fig. 3a), further confirming that four elements of Ni, Co, O, and C are contained in composites [36]. The Ni 2p emission spectrum in Fig. 3b is matched up two characteristic spin–orbit doublets of Ni^{3+} and Ni^{2+} as well as two shakeup satellites relying on the Gaussian fitting method. The fitting peaks at 874.9 eV and 856.9 eV, and other two peaks at 873.4 eV and 855.7 eV are associated with Ni^{3+} and Ni^{2+}, respectively. The two satellite peaks are observed at 879.4 eV and 861.5 eV, see attribution to the Ni $2_{p1/2}$ and Ni $2_{P3/2.}$ In Co 2p spectra, the fitting peaks are observed at the binding energies of 795.5 eV and 780.4 eV, see ascription to Co^{3+}, Co $2p_{3/2}$ and Co $2p_{1/2}$, while other peaks at

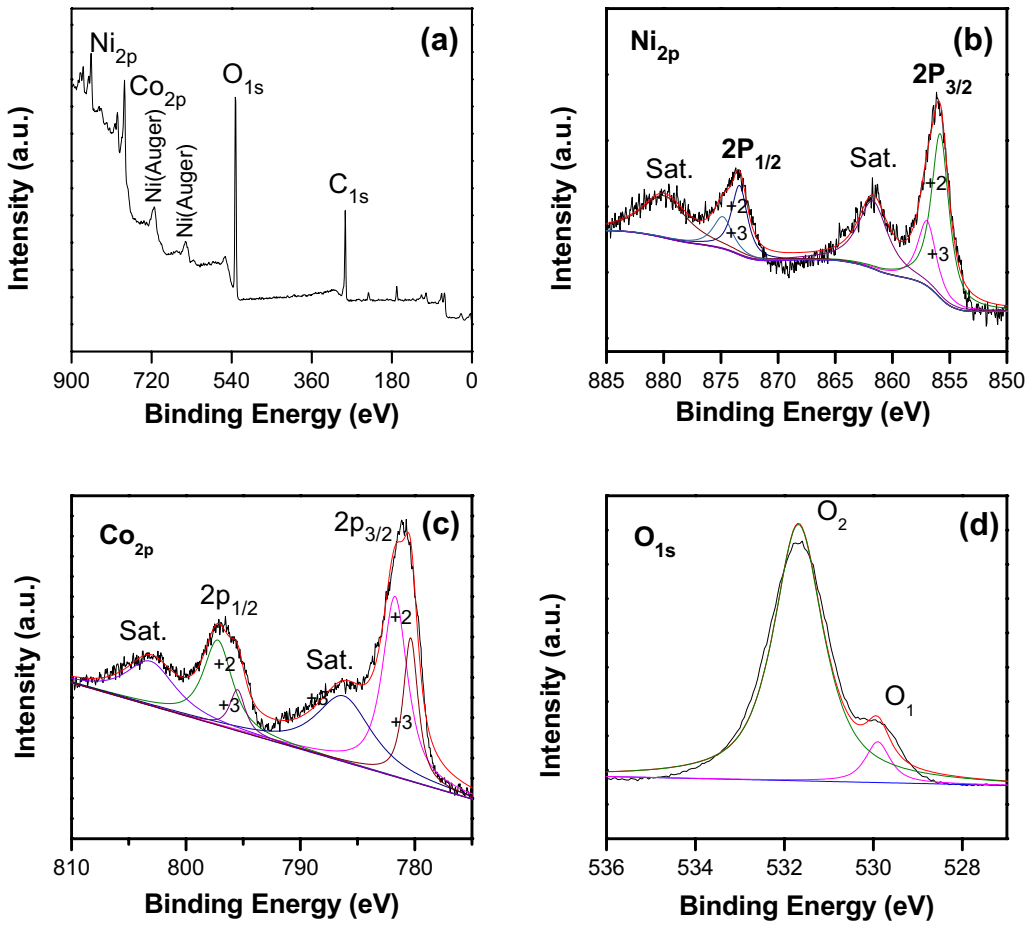

Fig. 3 **a** XPS full spectrum, **b** Ni 2P, **c** Co 2p, and **d** O 1s spectra of the CNT-$NiCo_2O_4$ composite

797.2 eV and 781.7 eV can be indexed to Co^{2+} (Fig. 3c) [37]. According to these XPS results, the as-prepared CNT-$NiCo_2O_4$ composites exhibit a rich oxidation state distribution including Ni^{3+}, Ni^{2+}, Co^{3+} , and Co^{2+}, which are beneficial for high electrochemical performance. The O 1 s fitting peaks in Fig. 3d indicates only two contributions, which are attributed to O 1 at the binding energy of 529.9 eV and O 2 at 531.7 eV. Specifically, the binding energy at the 529.9 eV is denoted as metal–oxygen (M–O) bond, while the other peak at the 531.7 eV presents a general relation to the oxygen in hydroxyl groups, defects, and chemically or physically absorbed water on the surface of composite [38].

FESEM was applied to studying the as-synthesized samples regarding their morphologies. 10–20 nm smooth walls with a length of dozens micrometers of the pristine CNTs are displayed in Fig. 4a. After hydrothermal disposed in a solution comprising Ni ion and Co ion coupled with calcination, CNTs were decorated by many $NiCo_2O_4$ nanoparticles, (Fig. 4b, c). The interconnected 3D structure of CNT is well-covered $NiCo_2O_4$ nanoparticles from low magnification SEM in Fig. 4b. From higher magnification SEM in Fig. 4c, it is distinct that smooth CNTs are decorated with ultrafine $NiCo_2O_4$ nanoparticles, which make the composites high conductivity and large surface.

Figure 5a and 5b manifests the CNT-$NiCo_2O_4$ in terms of their corresponding TEM images. Obviously, CNTs are covered with ultrafine $NiCo_2O_4$ nanoparticles, which are in good agreement with the SEM results. At a higher magnification in Fig. 5c, the spacing between contiguous fringes is ca. 0.35 nm, which corresponds to the CNT plane (002), consistent with the XRD result of CNT. It can be observed that an obvious set of lattice fringes of which the inter-planar spacing reached 0.2 nm, attributing to spinel $NiCo_2O_4$ the (400) plane, which further confirm the XRD result of $NiCo_2O_4$. Figure 5e–h reveals elemental distribution of composite, corresponding to elemental color mapping of C, Ni, Co, and O, respectively. This results further confirming the successful fabrication of the CNT-$NiCo_2O_4$ composites [39].

A configuration with three electrodes in 3 M KOH aqueous solution helped to evaluate the CNT-$NiCo_2O_4$ electrode with regard to electrochemical properties. Figure 6a describes cyclic voltammetric (CV) curves of CNT, pure $NiCo_2O_4$, as well as CNT-$NiCo_2O_4$ hybrid sample at a certain scan rate (5 mV s^{-1}). It is obvious that there is a pair of intense redox peaks for CNT-$NiCo_2O_4$ and $NiCo_2O_4$, manifesting that faradaic reactions mainly dominate the electrode in terms of the specific capacitance. The CV negligible integrated area of CNT suggests that CNTs contribute barely to hybrid electrodes regarding the specific capacitance. In summary, the CNT-$NiCo_2O_4$ hybrid material possesses the large integrated area compared with pure $NiCo_2O_4$ and CNT.

Representative CV curves of CNT-$NiCo_2O_4$ hybrid nanoparticles at different scan rates in 5–50 mV.s^{-1} are displayed in Fig. 6b. Obviously, a pair of redox peaks can be observed in the potential window in the range of 0–0.4 V vs. SCE. The peaks were considered a primary attribution to the redox reactions associated with M–O/M–O–OH, where M denotes Ni or Co ions. The relevant redox reaction may be given as below [40]:

$$NiCo_2O_4 + OH^- + H_2O \leftrightarrow NiOOH + 2CoOOH + e^-$$

It is noting that the redox peaks shifted toward lower potential and higher potential with the increase in scan rate, respectively, which may be ascribed to the electron transfer kinetics as the restricted step of redox reaction [41].

The specific capacitance of CNT-$NiCo_2O_4$ electrode was further estimated by the measurement of galvanostatic charge–discharge (GCD), with 0–0.4 V vs. SCE and different current densities in the range of 1–20 A g^{-1} (Fig. 6c). The voltage plateaus are in agreement with the redox peaks indicated in CV curves, which further demonstrates the pseudocapacitive behavior of hybrid nanomaterials. The specific capacitance exhibited by CNT-$NiCo_2O_4$ hybrid electrode material was evaluated from GCD curves based on formula $C = I\Delta t/m\Delta V$, thereinto, I denotes current of charge–discharge, Δt denotes discharge time, m refers to

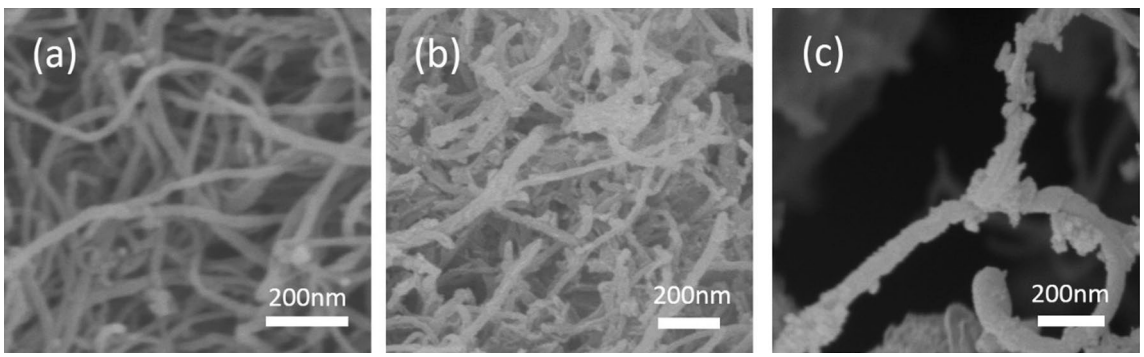

Fig. 4 SEM images of **a** pristine CNT, **b**, **c** CNT-$NiCo_2O_4$ composite

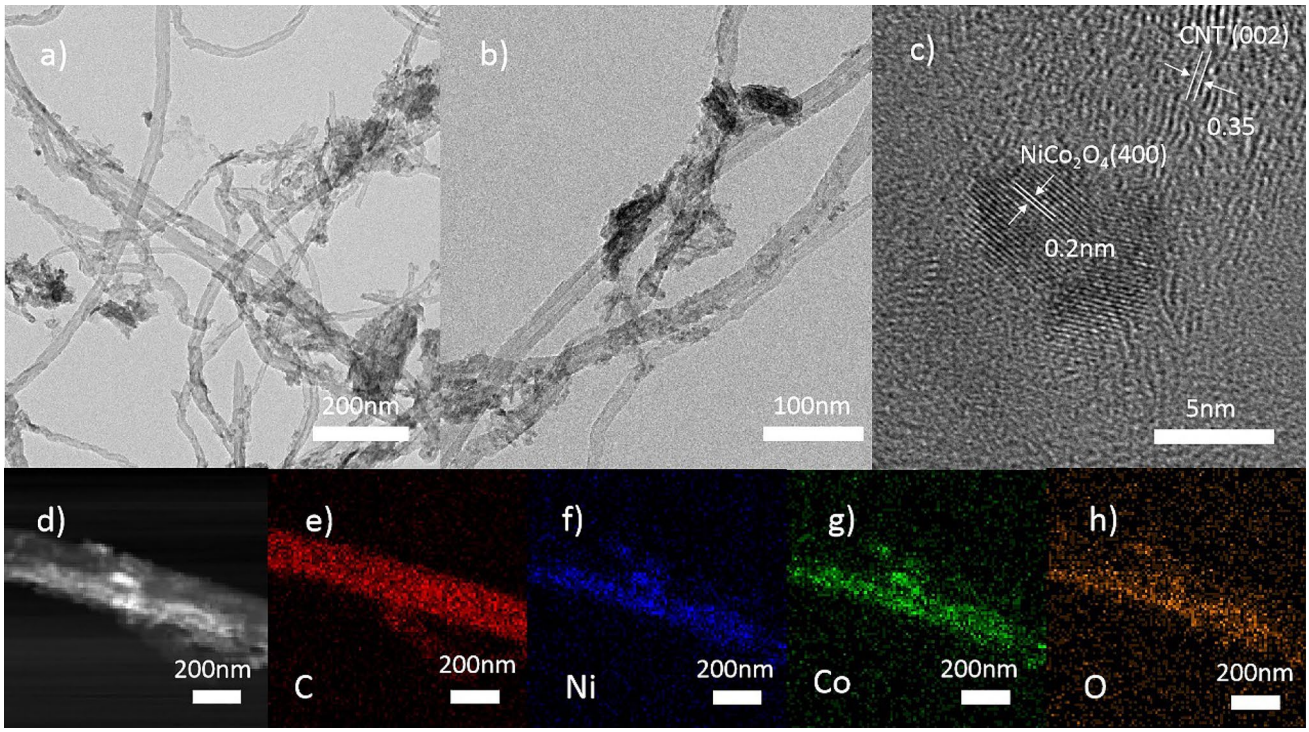

Fig. 5 **a**, **b**, **d** TEM of the as-synthesized compound, **c** high-resolution TEM images of the composite, **e**, **f** elemental mapping of the CNT-$NiCo_2O_4$

most active materials, and ΔV refers to the voltage change of GCD process [42]. According to the formula, specific capacitances (C) of CNT-$NiCo_2O_4$ calculated to be 1055 F g^{-1}, 1049 F g^{-1}, 1024 F g^{-1}, 998 F g^{-1} , and 950 F g^{-1} at current density of 1 A g^{-1}, 2 A g^{-1}, 5 A g^{-1}, 10 A g^{-1} , and 20 A g^{-1}, respectively.

Moreover, rate capability of CNT, pure $NiCo_2O_4$, and different concentration of CNT-$NiCo_2O_4$ was evaluated within the current density in the range of 1–20 A g^{-1} (Fig. 6d). CNT-$NiCo_2O_4$, amount of SDS is 18 mg L^{-1}, possesses larger rate capability compared with other samples. This result is attributed to appropriate amount of SDS. A small amount of SDS is not effective, but the excessive SDS may increase the size of $NiCo_2O_4$ particles (Fig. S1). The GCD test results indicate that about 90% of the capacitance for hybrid electrode is still remained when current density of the charge–discharge presents an increase in the range of 1–20 F g^{-1}. As we can say, this kind of ultrahigh electrochemical performance is barely reported for the composite of CNT-$NiCo_2O_4$, which is ascribed to the profitable of structure. Concretely, one-dimensional CNT wrapping each other to form a structure of network, as a conductive substrate, have strong contact with $NiCo_2O_4$ nanoparticles, which give rise to very considerable surface area.

Compared with CNT and pure $NiCo_2O_4$ electrode, the CNT-$NiCo_2O_4$ hybrid electrodes demonstrate a better electrochemical advantage in views of specific capacitance together with rate capability. For clarifying this reason, the electrochemical impedance analysis of all samples with frequency in 100–0.01 Hz with 5 mV amplitude is measured, as depicted in Fig. 6e. The EIS data were fitted by an equivalent circuit shown in the inset of Fig. 6e, where the R_s is the bulk solution resistance, R_{ct} is the Faradaic charge transfer resistance, CPE is a constant phase element, C_p is pseudocapacitive element, CPE is a constant phase element, and C_L is the inductance capacitance [43]. Obviously, the two electrodes show similar Nyquist plots, both composed of a semicircle with a small diameter and a straight line in region with high and low frequency, respectively. The solution resistance (R_s) and charge transfer resistance (R_{ct}) are calculated from Nyquist plots of the EIS spectra. It can be estimated that CNT-$NiCo_2O_4$ electrode exhibits a lower R_{ct} (0.17 Ω) and a lower R_s (0.57 Ω) compared with pure $NiCo_2O_4$ electrode (R_{ct} 0.36 and R_s 0.72), suggesting the ability of composite electrode to offer a faster pathway for the ion and electron transports during redox reactions. Moreover, the CNT-$NiCo_2O_4$ hybrid electrode shows a more steep line in region with low frequency compared with pure $NiCo_2O_4$.This result manifests better capacitive performance and fast electrolyte ion diffusion compared with pure $NiCo_2O_4$, which is in a good agreement with electrochemical test. The CNT anchored by $NiCo_2O_4$ particles composite

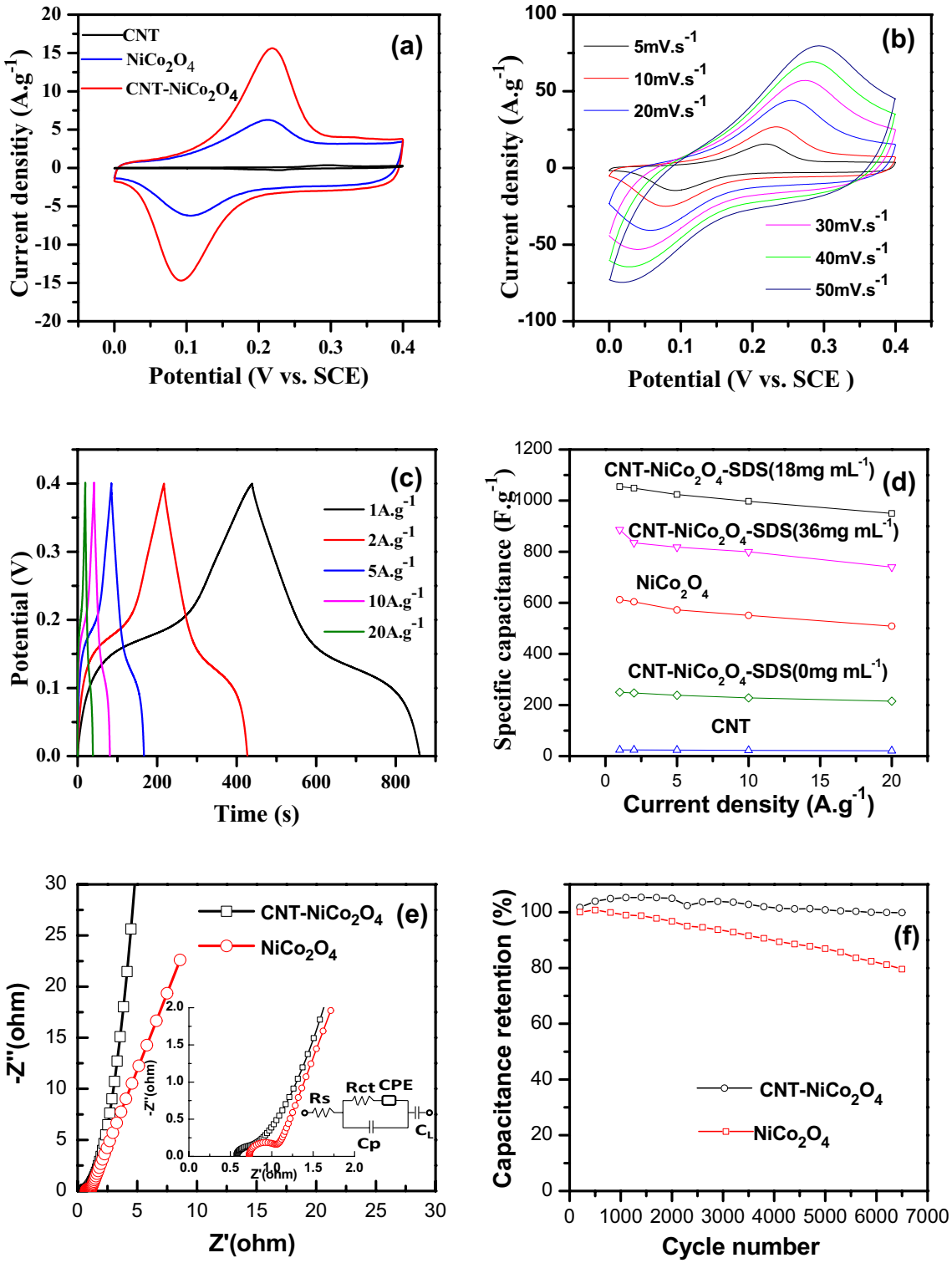

Fig. 6 **a** CV curves of the CNT, $NiCo_2O_4$, and CNT-$NiCo_2O_4$ electrodes obtained at 5 mV s^{-1} scan rate. **b** CV curves of the CNT-$NiCo_2O_4$ composite collected at distinct scan rates. **c** GCD curves of CNT-$NiCo_2O_4$ at different current densities. **d** Specific capacitances of all samples as a function of current densities. **e** Electrochemical impedance spectra (EIS) of the $NiCo_2O_4$ and CNT-$NiCo_2O_4$ electrodes. **f** Cyclic performance (at 20 A g^{-1} current density) of $NiCo_2O_4$ and CNT-$NiCo_2O_4$

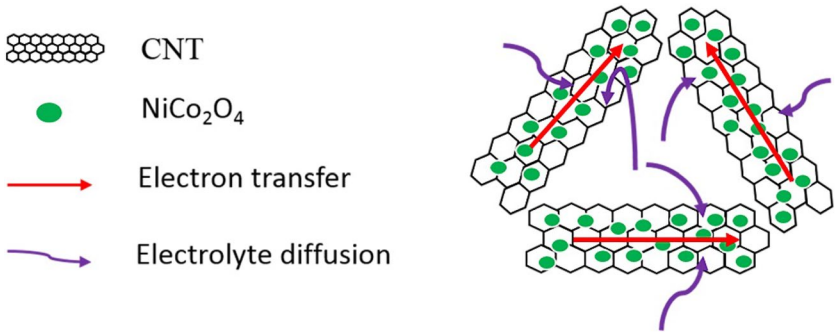

Fig. 7 Schematic illustration of the charge storage process of CNT-$NiCo_2O_4$ composite electrodes

with high conductivity could ensure better electrolyte accessibility together with fast charge transfer process compared with pure $NiCo_2O_4$, therefore improving its electrochemical performance.

The cycling property of the CNT-$NiCo_2O_4$ and the $NiCo_2O_4$ as another critical factor for supercapacitor practical applications was measured at a constant charge/discharge current densities (20 A g^{-1}) for 6500 cycles, as depicted in Fig. 6f. Obviously, specific capacitance of CNT-$NiCo_2O_4$ presents a gradual increase during original cycles instead of decreasing as in most cyclic performance tests, ascribed to the entire process to activate electrode material. This situation has also been recorded by some research groups [44]. The CNT-$NiCo_2O_4$ electrode maintains 99.8% of the initial specific capacitance, which is higher than the pure $NiCo_2O_4$ with 79.6% retention, indicating hybrid electrode remarkable cycling stability. The excellent cycling performance is attributed to the effective combination of highly conductive CNT and $NiCo_2O_4$. This unique structure will not be damaged during the electrochemical reaction. Significantly, the existence of CNT plays a crucial role in enhancing cycling lifespan of composite.

Considering the above discussion, it is noting that ultrahigh electrochemical performance of CNT-$NiCo_2O_4$ composite can be attributed to CNT-$NiCo_2O_4$ with unique three-dimensional structure. Figure 7 shows that electron transfer and electrolyte diffusion process of CNT-$NiCo_2O_4$ composite electrodes. The high conductivity CNT accelerates electron transfer and shortens the transport path for ion and electrolyte during the electrochemical reaction.

4 Conclusions

In this paper, a new method was developed. SDS was used as a dispersant and surfactant for CNT and precursor of composite was annealed to prepare CNT-$NiCo_2O_4$ hybrid material, so that ultrafine $NiCo_2O_4$ nanoparticles were firmly fixed on the surface of CNT. Consequently, the mixed structure could provide both excellent conductivity and large surface for achieving excellent electrochemical performance of supercapacitors. The synergistic effect generated by the favorable conductivity of CNT with large surface and the ultrahigh theoretic specific capacitance of $NiCo_2O_4$ achieves admirable cycling stability. Specifically, the electrode material barely decreased after 6500 cycles of charge–discharge at 20 A g^{-1} and high specific capacitance demonstrates ultrahigh capacitance of 1055 F g^{-1} at 1 A g^{-1} as an electrode material for supercapacitors. This ultrahigh performance makes the composite a promising candidate for supercapacitor electrode, and this research provides a novel method for preparing CNT-$NiCo_2O_4$ composite.

References

1. J. Guo, Z. Yin, X. Zang, Z. Dai, Y. Zhang, W. Huang, X. Dong, Facile one-pot synthesis of $NiCo_2O_4$ hollow spheres with controllable number of shells for high-performance supercapacitors. Nano Res. **10**, 405–414 (2017)
2. M. Azadfalah, A. Sedghi, H. Hosseini, Synergistic effect of Ni-based metal organic framework with graphene for enhanced electrochemical performance of supercapacitors. J. Mater. Sci. **30**, 12351–12363 (2019)
3. H. Chen, J. Jiang, L. Zhang, T. Qi, D. Xia, H. Wan, Facilely synthesized porous $NiCo_2O_4$ flowerlike nanostructure for high-rate supercapacitors. J. Power Sources **248**, 28–36 (2014)
4. Y. Zhu, X. Ji, Z. Wu, W. Song, H. Hou, Z. Wu, X. He, Q. Chen, C.E. Banks, Spinel $NiCo_2O_4$ for use as a high-performance supercapacitor electrode material: understanding of its electrochemical properties. J. Power Sources **267**, 888–900 (2014)
5. R. Zou, K. Xu, T. Wang, G. He, Q. Liu, X. Liu, Z. Zhang, J. Hu, Chain-like $NiCo_2O_4$ nanowires with different exposed reactive planes for high-performance supercapacitors. J. Mater. Chem. A **1**, 8560 (2013)
6. S. Gao, Y. Sui, F. Wei, J. Qi, Q. Meng, Y. Ren, Y. He, Dandelion-like nickel/cobalt metal-organic framework based electrode materials for high performance supercapacitors. J. Colloid Interface Sci. **531**, 83–90 (2018)
7. H. Wang, J. Lu, S. Yao, W. Zhang, Sodium dodecyl sulfate-assisted synthesis of flower-like $NiCo_2O_4$ microspheres with large specific surface area for supercapacitors. J. Alloy Compd. **744**, 187–195 (2018)
8. F. Huang, Y. Sui, F. Wei, J. Qi, Q. Meng, Y. He, Ni_3S_4 supported on carbon cloth for high-performance flexible all-solid-state asymmetric supercapacitors. J. Mater. Sci. Mater. Electron. **29**, 2525–2536 (2017)

9. B. Li, Q. Sun, R. Yang, D. Li, Z. Li, Simple preparation of graphene-decorated $NiCo_2O_4$ hollow nanospheres with enhanced performance for supercapacitor. J. Mater. Sci. Mater. Electron. **29**, 7681–7691 (2018)
10. Y. Zhu, Z. Wu, M. Jing, W. Song, H. Hou, X. Yang, Q. Chen, X. Ji, 3D network-like mesoporous $NiCo_2O_4$ nanostructures as advanced electrode material for supercapacitors. Electrochim. Acta **149**, 144–151 (2014)
11. C. Yuan, J. Li, L. Hou, X. Zhang, L. Shen, X.W.D. Lou, Ultrathin mesoporous $NiCo_2O_4$ nanosheets supported on Ni foam as advanced electrodes for supercapacitors. Adv. Funct. Mater. **22**, 4592–4597 (2012)
12. G. Zhang, X.W. Lou, General solution growth of mesoporous $NiCo_2O_4$ nanosheets on various conductive substrates as high-performance electrodes for supercapacitors. Adv. Mater. **25**, 976–979 (2013)
13. T.H. Ko, S. Radhakrishnan, W.K. Choi, M.K. Seo, B.S. Kim, Core/shell-like $NiCo_2O_4$-decorated MWCNT hybrids prepared by a dry synthesis technique and its supercapacitor applications. Mater. Lett. **166**, 105–109 (2016)
14. S. Xu, D. Yang, F. Zhang, J. Liu, A. Guo, F. Hou, Fabrication of $NiCo_2O_4$ and carbon nanotube nanocomposite films as a high-performance flexible electrode of supercapacitors. RSC Adv. **5**, 74032–74039 (2015)
15. Y. Zheng, Z. Lin, W. Chen, B. Liang, H. Du, R. Yang, X. He, Z. Tang, X. Gui, Flexible, sandwich-like CNTs/$NiCo_2O_4$ hybrid paper electrodes for all-solid state supercapacitors. J. Mater. Chem. A **5**, 5886–5894 (2017)
16. S. Gao, Y. Sui, F. Wei, J. Qi, Q. Meng, Y. He, Facile synthesis of cuboid Ni-MOF for high-performance supercapacitors. J. Mater. Sci. **53**, 6807–6818 (2018)
17. S. Bose, T. Kuila, A.K. Mishra, R. Rajasekar, N.H. Kim, J.H. Lee, Carbon-based nanostructured materials and their composites as supercapacitor electrodes. J. Mater. Chem. **22**, 767–784 (2012)
18. Y. Yao, C. Ma, J. Wang, W. Qiao, L. Ling, D. Long, Rational design of high-surface-area carbon nanotube/microporous carbon core-shell nanocomposites for supercapacitor electrodes. ACS Appl. Mater. Interfaces **7**, 4817–4825 (2015)
19. K. Shree Kesavan, K. Surya, M.S. Michael, High powered hybrid supercapacitor with microporous activated carbon. Solid State Ion. **321**, 15–22 (2018)
20. N. Kumar, Y.-C. Yu, Y.H. Lu, T.Y. Tseng, Fabrication of carbon nanotube/cobalt oxide nanocomposites via electrophoretic deposition for supercapacitor electrodes. J. Mater. Sci. **51**, 2320–2329 (2015)
21. F. Cai, Y. Kang, H. Chen, M. Chen, Q. Li, Hierarchical CNT@$NiCo_2O_4$ core–shell hybrid nanostructure for high-performance supercapacitors. J. Mater. Chem. A **2**, 11509–11515 (2014)
22. S. Ramesh, D. Vikraman, H.S. Kim, H.S. Kim, J.H. Kim, Electrochemical performance of MWCNT/GO/$NiCo_2O_4$ decorated hybrid nanocomposite for supercapacitor electrode materials. J. Alloy Compd. **765**, 369–379 (2018)
23. S. Zhang, H. Gao, J. Zhou, F. Jiang, Z. Zhang, Hydrothermal synthesis of reduced graphene oxide-modified $NiCo_2O_4$ nanowire arrays with enhanced reactivity for supercapacitors. J. Alloy Compd. **792**, 474–480 (2019)
24. H.C. Xuan, Y.K. Xu, Y.Q. Zhang, H. Li, P.D. Han, Y.W. Du, One-step combustion synthesis of porous CNTs/C/$NiMoO_4$ composites for high-performance asymmetric supercapacitors. J. Alloy Compd. **745**, 135–146 (2018)
25. M. Shahraki, S. Elyasi, H. Heydari, N. Dalir, Synthesis of carbon-based spinel $NiCo_2O_4$ nanocomposite and its application as an electrochemical capacitor. J. Electron. Mater. **46**, 4948–4954 (2017)
26. X. Zhou, A.Q. Wang, Y.M. Pan, C.F. Yu, Y. Zou, Y. Zhou, Q. Chen, S.S. Wu, Facile synthesis of a Co_3O_4@carbon nanotubes/polyindole composite and its application in all-solid-state flexible supercapacitors. J. Mater. Chem. A **3**, 13011–13015 (2015)
27. L. Geng, S.S. Xu, J.C. Liu, A.R. Guo, F. Hou, Effects of CNT-film pretreatment on the characteristics of $NiCo_2O_4$/CNT core-shell hybrids as electrode material for electrochemistry capacitor. Electroanalysis **29**, 778–786 (2017)
28. Y. Zhu, J. Chen, N. Zhao, W. Lin, C. Lai, Q. Wang, Large-scale synthesis of uniform $NiCo_2O_4$ nanoparticles with supercapacitive properties. Mater. Lett. **160**, 171–174 (2015)
29. X. Wang, Y. Yang, P. He, F. Zhang, J. Tang, Z. Guo, R. Que, Facile synthesis of MnO_2@$NiCo_2O_4$ core-shell nanowires as good performance asymmetric supercapacitor. J. Mater. Sci. Mater. Electron. **31**, 1355–1366 (2019)
30. J. Di, H.S. Xu, X.K. Gai, R.Q. Yang, H.J. Zheng, One-step solvothermal synthesis of feather duster-like CNT@WO_3 as high-performance electrode for supercapacitor. Mater. Lett. **246**, 129–132 (2019)
31. Y.F. Wang, S.X. Zhao, L. Yu, X.X. Zheng, Q.L. Wu, G.Z. Cao, Design of multiple electrode structures based on nano Ni_3S_2 and carbon nanotubes for high performance supercapacitors. J. Mater. Chem. A **7**, 7406–7414 (2019)
32. X.W. Chang, W.L. Li, Y.H. Liu, M. He, X.L. Zheng, X.Z. Lv, Z.Y. Ren, Synthesis and characterization of $NiCo_2O_4$ nanospheres/nitrogen-doped graphene composites with enhanced electrochemical performance. J. Alloy Compd. **784**, 293–300 (2019)
33. H. Wang, C. Shen, J. Liu, W. Zhang, S. Yao, Three-dimensional $MnCo_2O_4$/graphene composites for supercapacitor with promising electrochemical properties. J. Alloy Compd. **792**, 122–129 (2019)
34. L.C. Yue, S.G. Zhang, H.Q. Zhao, Y. Feng, M. Wang, L.L. An, X.D. Zhang, J. Mi, One-pot synthesis $CoFe_2O_4$/CNTs composite for asymmetric supercapacitor electrode. Solid State Ion. **329**, 15–24 (2019)
35. J.G. Kim, Y. Kim, Y. Noh, W.B. Kim, MnCo2O4 nanowires anchored on reduced graphene oxide sheets as effective bifunctional catalysts for Li-O2 battery cathodes. Chemsuschem **8**, 1752–1760 (2015)
36. L.B. Ma, X.P. Shen, H. Zhou, Z.Y. Ji, K.M. Chen, G.X. Zhu, High performance supercapacitor electrode materials based on porous $NiCo_2O_4$ hexagonal nanoplates/reduced graphene oxide composites. Chem. Eng. J. **262**, 980–988 (2015)
37. Q. Tang, Y. Zhou, L. Ma, M. Gan, Hemispherical flower-like N-doped porous carbon/$NiCo_2O_4$ hybrid electrode for supercapacitors. J. Solid State Chem. **269**, 175–183 (2019)
38. J. Bhagwan, G. Nagaraju, B. Ramulu, S.C. Sekhar, J.S. Yu, Rapid synthesis of hexagonal $NiCo_2O_4$ nanostructures for high-performance asymmetric supercapacitors. Electrochim. Acta **299**, 509–517 (2019)
39. Y.-R. Zhu, P.-P. Peng, J.-Z. Wu, T.-F. Yi, Y. Xie, S. Luo, Co_3O_4@$NiCo_2O_4$ microsphere as electrode materials for high-performance supercapacitors. Solid State Ion. **336**, 110–119 (2019)
40. X. Wang, X.D. Han, M. Lim, N. Singh, C.L. Gan, M. Jan, P.S. Lee, Nickel Cobalt Oxide-single wall carbon nanotube composite material for superior cycling stability and high-performance supercapacitor application. J. Phys. Chem. C **116**, 12448–12454 (2012)
41. D. Guo, H. Zhang, X. Yu, M. Zhang, P. Zhang, Q. Li, T. Wang, Facile synthesis and excellent electrochemical properties of $CoMoO_4$ nanoplate arrays as supercapacitors. J. Mater. Chem. A **1**, 7247 (2013)

42. W. Yu, B.Q. Li, S.J. Ding, Electroless fabrication and supercapacitor performance of CNT@NiO-nanosheet composite nanotubes. Nanotechnology **27**, 075605 (2016)
43. J. Xiao, S. Yang, Sequential crystallization of sea urchin-like bimetallic (Ni, Co) carbonate hydroxide and its morphology conserved conversion to porous $NiCo_2O_4$ spinel for pseudocapacitors. RSC Adv. **1**, 588–595 (2011)
44. C. Wang, X. Zhang, D. Zhang, C. Yao, Y. Ma, Facile and low-cost fabrication of nanostructured $NiCo_2O_4$ spinel with high specific capacitance and excellent cycle stability. Electrochim. Acta **63**, 220–227 (2012)